High-Frequency Winds and Eddy Resolving Models

Patrice Klein,[1]

Patrice Klein, Département d'Océanographie Physique et Spatiale, Ifremer Centre de Brest, BP 70, F-29280 Plouzané, France. (pklein@ifremer.fr)

[1]Laboratoire de Physique des Océans,

Ifremer, Plouzané, France

Abstract. Wind energy input to oceanic near-inertial motions (estimated between 0.5 TeraWatt (TW) and 0.9 TW) is comparable to the work done by the steady large-scale winds on the general circulation of the ocean (estimated to be 1 TW). This energy input is the largest principally in the regions of atmospheric storm tracks. It is one of the main kinetic energy sources that may sustain the small-scale mixing at depth that is necessary to maintain the deep ocean stratification and therefore to close the total kinetic energy budget. But how much of this wind-driven near-inertial energy penetrates into the deep ocean interior, and where, is still a puzzle. In other words, what is the route to mixing from the surface to the deep interior followed by these motions? In this review we present different pathways by which near-inertial energy ultimately can reach the deep interior and be available for mixing. The dominant pathway appears to be through the oceanic turbulent eddy fields at mid-latitudes. It makes a non-negligeable part of the near-inertial energy to penetrate into the deep interior with conspicuous maxima at depths as large as $2500-3000$ m. However, we still lack a precise quantification of the contribution of the different pathways and in particular of the part of near-inertial energy used for mixing the upper layers relatively to that used for mixing the deeper layers. Eddy-resolving models at a basin scale (with adequate spatial resolution) forced by high-frequency winds should be able in the close future to explicitly represent the 3-D propagation of the near-inertial waves down to 5000 m. A few process studies are still needed to parameterize mixing generated by these waves and in particular of those in the deep interior.

1. Wind ringing of the ocean at the near-inertial frequency

The ocean is a stratified rotating fluid and, as such, supports several classes of high-frequency waves from the Coriolis frequency (f) to the Brunt-Väisälä frequency. At mid-latitude, these frequencies range from 10^{-4}s^{-1} for the Coriolis frequency to 3.10^{-3}s^{-1} for the Brunt-Väisälä frequency. A classical dispersion relation for these waves (in the shallow water framework) is

$$\omega^2 = f^2(1 + k^2 r_d^2) \tag{1}$$

with ω the wave frequency, k their horizontal wave number and r_d a Rossby radius of deformation[1] that characterizes the oceanic stratification. Atmospheric wind stress can force these different classes of waves if wind energy is present in this large frequency band. However, high-frequency winds are characterized by wave number spectra that exhibit energetic horizontal scales of the order of $\mathcal{O}(500-1000$ km), i.e. much larger than the oceanic internal Rossby radii of deformation (< 50 km). This means that, for oceanic motions forced by such a wind stress, kr_d is much smaller than 1, which explains that the frequency of the resulting wind-driven waves is close to the Coriolis frequency. These near-inertial waves are trapped within the surface mixed-layer ($50-100$ m deep) and therefore the mixed-layer can be considered as an oscillator with the frequency f.

Winds are strongly intermittent in time with periods ranging from $3-6$ hours to much larger time scales. If the wind stress possesses some energy in the inertial frequency band and rotates in the same direction as the near-inertial motions, a systematic increase of the near-inertial kinetic energy and mixing will occur within the mixed-layer. Such a resonance mechanism has been well explained by several studies [e.g. *Klein and Coantic*, 1981; *Large and Crawford*, 1995; *Skyllinstad et al.*, 2000].

Figure 1 (from *Klein et al.* [2004a]) can help to explain the impact of the high-frequency winds and the associated resonance mechanism. It shows the time evolution of the wind intensity (in terms of u^{*3}) (upper panel), the wind energy flux (middle panel) (i.e. $\boldsymbol{\tau} \cdot \mathbf{u}$, with $\boldsymbol{\tau}$ the wind stress vector and $\mathbf{u}$ the surface velocity vector) and the integrated near-inertial energy (lower panel), obtained by using three hourly meteorological data sampled on the weathership "KILO" located in the North-Atlantic. Comparison of the upper and middle panels indicates that not all strong wind events produce a positive wind energy flux and therefore increase the kinetic energy. Actually a non-negligeable number of strong wind events decreases the kinetic energy, which illustrates the importance of the phase relationship between the wind stress direction and the surface velocity vector. A particular and conspicuous signature of this resonance mechanism is highlighted in tropical hurricane studies (see *Price* [1981] and *Price et al.* [1994]). They reveal that in the North Hemisphere this mechanism induces greater cooling on the right side of the hurricane trajectory (where, at a given point, winds rotate clockwise as the hurricane moves across) compared to the left side (where winds rotate anti-clockwise).

One interesting feature is that the evolution of the total kinetic energy (shown on the lower panel of Figure 1) is characterized by periods of persisting large amplitude (that last between 10 and 20 days) followed by periods of small amplitude. As found by previous studies [e.g. *Large and Crawford*, 1995; *Skyllinstad et al.*, 2000; *Klein et al.*, 2004a], not only the frequency (with respect to the Coriolis frequency) but also the rotation of the wind fluctuations is important for the resonance mechanism. Thus another experiment identical to the first one but with the Coriolis parameter having the opposite sign has revealed that although the magnitude of the kinetic energy averaged over 540 days is about the same, its time evolution (not shown) displays strong differences.

To better quantify the impact of the high-frequency wind fluctuations on the ocean ringing, the experiment reported in Figure 1 has been compared with others identical to this one but that use the wind stress averaged over 6, 12, and 24 hours. This impact is clearly revealed by Table 1: when the wind stress is averaged over 6, 12, and 24 hours, the total kinetic energy is decreased, respectively, by 1.5, 3, and 7! The resonance mechanism mentioned before also explains the near-inertial oscillations with large amplitude that are present in the in situ observations [e.g. *Stockwell et al.*, 2004]. All these results illustrate the necessity to use at least a 3-hourly wind time series to force the ringing of the ocean, i.e. to correctly estimate the wind energy flux to the ocean in the inertial frequency band.

2. High-frequency wind energy flux and the global oceanic circulation

Alford [2001], *Watanabe and Hibiya* [2002], and *Alford* [2003] indicate that the wind kinetic energy input to oceanic near-inertial motions is the largest principally in the regions of atmospheric storm tracks located at mid-latitudes, i.e. where the high-frequency winds are the strongest. These high-frequency winds are essentially linked to the extratropical cyclone frequency and intensity and their associated fast travelling atmospheric fronts. Plate 1a (from *Alford* [2003]) illustrates these results during the Northern Hemisphere winter: the excited near-inertial energy is the largest north of 30° latitude. During the Southern Hemisphere winter the largest energy input regions are south of 30° latitude. The seasonal variation of this wind energy input is much stronger in the Northern Hemisphere than in the Southern Hemisphere. These studies used data re-analysis from Meteorological National Centers (with usually a two-degree spatial resolution and a time interval of 6 hours). However, *Watanabe and Hibiya* [2002] and *Alford* [2003] have applied correction factors in order to get a better estimation of the wind-driven near-inertial motions when using such 6-hourly wind data. The ocean part is represented

only by a slab mixed-layer model and a Rayleigh damping is used to mimic the radiation of the near-inertial energy from the mixed-layer to the deeper ocean. There is no large or mesoscale oceanic circulation.

Contribution of this wind kinetic energy input to the global oceanic energy budget is discussed by *Wunsch and Ferrari* [2004]. Using *Alford* [2003]'s results, they found that the global energy input due to high-frequency winds (estimated between 0.5 TW and 0.9 TW) is comparable to the work done by the steady large-scale winds on the general circulation (estimated to be 1 TW). These numbers are probably underestimated because of the low spatial resolution of the meteorological data used (see section 6). However the importance, for the dynamics of the general oceanic circulation, of this large amount of energy input to the near-inertial waves is clearly invoked by *Munk and Wunsch* [1998] and *Wunsch and Ferrari* [2004]. They suggest that the resulting wind-driven near-inertial energy could sustain the small-scale mixing in the deep interior that is necessary to resupply the available potential energy removed by mesoscale eddy generation and the Meridional Overtuning Circulation (MOC). Thus high-frequency winds may provide enough energy to maintain the deep ocean stratification, in particular at mid-latitudes.

Alford [2003] notes that the total high-frequency wind energy input has increased by 28% since 1948. So assuming that these wind-forced near-inertial motions are a potential source of mechanical energy available for mixing in the deep ocean, then, using *Munk and Wunsch* [1998] and *Wunsch and Ferrari* [2004] arguments, a secular increase in extratropical atmospheric cyclone frequency and intensity would be accompanied by a strengthened MOC and/or an intensified eddy kinetic energy at mid-latitudes. The consequence of this comment is that the impact of the resulting mixing in the oceanic circulation cannot be parameterized as just

a constant global diffusion coefficient. This impact may be considered as a component of the coupled atmosphere-ocean system.

However, how much of this wind-driven near-inertial energy penetrates into the deep ocean interior, and where, is still a real puzzle. We need to better understand the mechanisms through which the near-inertial energy produced at the surface propagates downward. In other words, the question is, what is the detailed route to mixing from the surface to the deep interior followed by these motions? Some clues and suggestions for answering this question are offered in the next sections.

3. Downward and equatorward propagation of near-inertial energy due to the β-effect

Near-inertial motions may spread both horizontally and vertically into the interior, but only when their horizontal scale is small enough [e.g. *Gill*, 1984], in fact much smaller than the wind scales. This requires mechanisms to significantly reduce the initially large scales of these wind-driven motions. This is the first condition for the existence of a route to mixing from the surface to the deep interior.

Within this context, one of the promising directions to consider is the β-effect [e.g. *D'Asaro*, 1989]. It makes the near-inertial motions generated at mid-latitudes have much smaller horizontal scales than the wind scales, which can be illustrated from the following example. Using $f = f_0 + \beta y$, the near-inertial motions are written as

$$u(y,t) = u_o \sin(ft) = u_o \sin(f_0 t - ly); \tag{2}$$

with u_o a constant and $l = -\beta t$ [e.g. *Kunze*, 1985]. t is the time. Thus near-inertial waves are characterized by a meridional wave number l that grows with time, which make them reach a length scale of 100 km within at least a month. Such length scale reduction subsequently allows

them to propagate vertically in the interior [e.g. *Gill*, 1984]. Furthermore, since this meridional wave number is negative, these waves also freely propagate equatorward [e.g. *D'Asaro*, 1989; *Garrett*, 2001].

When these near-inertial waves propagating equatorward attain a critical latitude (defined as the latitude where their frequencies are twice the local Coriolis frequency), then a large part of their energy may be transferred down to small dissipation scales. Such processes occur through the well-known parametric subharmonic instability (PSI) [e.g. *Staquet and Sommeria*, 2002] that transfers energy across the local internal wave spectrum by nonlinear interactions amongst internal waves. A large amount of the near-inertial energy generated at mid-latitudes by high-frequency winds is then expected to be available for diapycnal mixing at these low latitudes (lower than $30°$N). Numerical experiments indicate that PSI is a much more effective mechanism than previously thought (involving a time scale of days instead of weeks or months) for transferring high-frequency energy (inertial and also tidal) to small dissipation scales [e.g. *Hibiya et al.*, 1998, 1999; *Nagasawa et al.*, 2000; *MacKinnon and Winters*, 2005].

Such a direction of investigation that involves the planetary vorticity gradient is appropriate for the global circulation models that do not resolve the mesoscales. However, it should be modified and eventually extended when higher numerical resolutions are considered, such as in eddy-resolving models.

4. Downward propagation of near-inertial energy in mesoscale eddies

Since *Weller* [1982], it has been recognized that mesoscale eddies (with a diameter between 50 km and 200 km) can distort the near-inertial motions and quickly decrease their length scales down to values smaller than 50 km within a few days [e.g. *Kunze*, 1985; *Van Meurs*, 1998]. *Kunze* [1985] argued that near-inertial waves propagating in geostrophic shear are subject not

only to the planetary vorticity gradient but principally to the absolute vorticity gradient, i.e. the gradient including the eddy vorticity effects. The eddy vorticity amplitude at mid-latitude can reach root-mean-square (rms) values as large as $0.3\ f$ and may involve scales as small as $5-20$ km [e.g. *Capet et al.*, 2007a; *Klein et al.*, 2007b]. This means that relative vorticity gradients associated with mesoscale eddies can be larger than β and therefore be a much more efficient mechanism to generate small scales. Another major difference with the β-effect is that near-inertial motions distorted by mesoscale eddies do not propagate equatorward. Instead they are "polarized" by eddies and more specifically, are expelled from cyclonic eddies and trapped within anti-cyclonic ones [e.g. *Kunze*, 1985; *D'Asaro*, 1995; *Young and Ben Jelloul*, 1997; *Klein et al.*, 2004b].

All these characteristics can be explained by considering the simple situation of Figure 2 that involves a meridional geostrophic jet. Inertial motions feel the rotation of the Earth but also feel the rotation of the mesoscale structures even when the latter is one order of magnitude smaller than the former. Hence, using a first-order Taylor series expansion for the mesoscale vorticity Z (i.e. $Z = Z_o + \boldsymbol{\nabla}\mathrm{Z} \cdot \boldsymbol{x} + ...$), near-inertial velocity can be written as

$$u(\boldsymbol{x}, t) \approx u_o \sin(ft + \frac{Z}{2}t) \approx u_o \sin(ft + \frac{Z_o}{2}t - \boldsymbol{k} \cdot \boldsymbol{x}); \tag{3}$$

with $\boldsymbol{k} = -\frac{t}{2}\boldsymbol{\nabla}\mathrm{Z}$, a wave number increasing with time [e.g. *Kunze*, 1985]. ∇ is the horizontal gradient operator and $\boldsymbol{x} = [x, y]$ with x and y respectively the zonal and meridional coordinates. Thus, as β, mesoscale vorticity gradients reduce the horizontal scales of the near-inertial motions. When $|\boldsymbol{\nabla}\mathrm{Z}| >> \beta$, this reduction may occur within a scale of a few days instead of months. Furthermore, these motions subsequently propagate but, as illustrated in Figure 2, the sign of $\boldsymbol{k}$ is such that they are expelled from cyclonic structures and are trapped within anti-cyclonic ones. Consequence of the near-inertial motion distortion by the eddy vorticity and their

subsequent horizontal propagation (proportional to the group velocity $C_g = f r_d^2 k / \sqrt{1 + r_d^2 k^2}$ obtained using equation (1)) is that these motions are first trapped within structures of the eddy Laplacian vorticity, i.e. $\nabla^2 Z$, (this is what Figure 2 shows), and then they overshoot this region to spread out within the larger eddy stream function structures. These two limits have been analyzed in *Klein and Tréguier* [1995]; *Young and Ben Jelloul* [1997]; *Balmforth et al.* [1998] and are identified as the weak dispersion limit and the strong dispersion limit.

The preceding discussion applies to the horizontal heterogeneity of near-inertial motions associated with one vertical mode. The vertical propagation of these motions within an eddy field can be understood when they involve several vertical normal modes [e.g. *Gill*, 1984]. Indeed, if lower and higher baroclinic modes have the same spatial variability and are initially in phase such that they add up within the mixed-layer and cancel out below (with the result of no motion there), then the vertical propagation of the near-inertial motions simply results from the phase decoupling of the different baroclinic modes. Let us introduce the time scale t_{dn} (following *Gill* [1984]) for a 180° phase difference to develop for mode n (using equation (1)),

$$t_{dn} = \frac{\pi}{\omega_n - f} \approx \frac{2\pi}{f k^2 r_{dn}^2} \, , \tag{4}$$

with ω_n and r_{dn} respectively the frequency of the near-inertial motions and the Rossby radius of deformation, both associated with the mode n. Then from equation (4), the lower modes (with large r_{dn}) first become out-of-phase with the higher ones (with small r_{dn}), and then the intermediate modes in turn become out-of-phase. The consequence of this phase decoupling is the emergence of non-zero motions at depth. This dynamic of the vertical modes strongly emphasizes the importance of the mechanisms described before (that reduce the length scale of the near-inertial motions) for the propagation of the near-inertial energy into the ocean interior [e.g. *Gill*, 1984].

Most of the related studies have considered isolated geostrophic eddies or jets characterized by only one specific length scale. In this case, a Wentzel-Kramer-Brillouin (WKB) analysis can help to understand the 3-D propagation of the near-inertial motions in the ocean. However, dispersion properties are quite different for a fully turbulent eddy field (involving strongly interacting eddies characterized by a continuous velocity spectrum). Such properties can be retrieved by using the methodology proposed by *Young and Ben Jelloul* [1997] that discards the WKB approximation and therefore allows any eddy structure, either large or small, to affect the distortion of the near-inertial motions. Extending the results of *Young and Ben Jelloul* [1997], *Klein et al.* [2004b] show that considering a fully turbulent eddy field leads to very different consequences for the behavior of the vertical modes: lower modes are trapped within structures with relatively large scales whereas higher modes are trapped within anti-cyclonic structures with much smaller scales. As a result of these differences in the spatial heterogeneity, the lower modes decouple more quickly from the higher ones and the resulting vertical propagation is therefore much faster and deeper.

5. Which pathway prevails?

We may wonder which dynamics principally drive the 3-D propagation, in the global ocean, of the large amount of near-inertial energy produced by the high-frequency winds.

We have mentioned before that atmospheric storm tracks at mid-latitudes are the regions where the wind energy input to the ocean at near-inertial frequencies is the strongest [e.g. *Alford*, 2001; *Watanabe and Hibiya*, 2002; *Alford*, 2003]. In global oceanic models, when mesoscale eddies are not fully resolved, near-inertial waves are usually produced near the surface at mid-latitudes and subsequently propagate equatorward and downward [*Komori*, 2007; *Sasaki*, 2007].

In these simulations the β-effect is the main mechanism that governs the 3-D propagation of these waves toward the Equator [e.g. *Nagasawa et al.*, 2000; *Garrett*, 2001].

However, as noticed by *Zhai et al.* [2005], the regions of high-frequency wind energy input are also those where the mesoscale eddy activity is the most energetic. This feature is illustrated by Plate 1, which shows that regions in the North Hemisphere of strong high-frequency wind energy fluxes (Plate 1a) coincide well with the locations of the Gulf Stream and the Kuroshio (Plate 1b). In the Southern Hemisphere, the high-frequency wind energy fluxes during the winter are principally at the same latitude as the Antarctic Circumpolar Current. Such remarkable coincidence indicates that much of the near-inertial energy produced by the high-frequency winds would be trapped within the oceanic mesoscale eddies. The polarization of near-inertial energy by mesoscale eddies should strongly compete with that induced by the β-effect.

One question is: Do these energetic eddy regions mostly concern isolated eddies or a fully turbulent eddy field. Considering eddies as just an ensemble of isolated structures was pertinent when observational data indicated a wave number velocity spectrum with a slope equal or even steeper than k^{-4} (although they may weakly interact [e.g. *Klein*, 1990]). However studies of the last seven years significantly strengthen the vision of an upper ocean crowded with a large number of strongly interacting eddies. Numerical experiments of *Hurlburt and Hogan* [2000] and *Siegel et al.* [2001] in the North Atlantic basin show that using a horizontal resolution of 1/64° leads to an explosion of eddies and to an eddy kinetic energy increase by a factor of 10 compared with classical "eddy-resolving models" (with a 1/6° resolution). Furthermore, they reveal that such fully turbulent eddy fields are not only present in well-known "eddy regions" such as the Gulf Stream or the Antarctic Circumpolar Current, but also in a large number of other regions. This corroborates the visual picture provided by the high-resolution satellite images as

well as some in situ data [e.g. *Stammer*, 1997; *Wunsch*, 1998; *Rudnick*, 2001; *Assenbaum and Reverdin*, 2005; *LeCann et al.*, 2005].

These comments strongly suggest that turbulent eddy fields at mid-latitudes are the prevailing pathways for the 3-D propagation of near-inertial waves. But we still lack a precise quantification of the contribution of these different pathways at a basin scale.

6. The route to mixing through eddy fields: some results

Several numerical studies have described the horizontal and vertical propagation of the near-inertial motions through interacting mesoscale eddies. In a low resolution ($1/3^\circ$) Southern ocean model, *Zhai et al.* [2005] show that the leakage of the near-inertial energy out of the 50 m deep mixed-layer is strongly enhanced by the presence of eddies. Their results point out a maximum of the horizontal near-inertial energy at a depth of 500 m. They also support the findings of *Lee and Niiler* [1998] indicating that anti-cyclonic eddies act as a conduit draining near-inertial energy to the deeper ocean (the "chimney effect"). Using a fully turbulent eddy field and a resolution of $1/15^\circ$, *Danioux et al.* [2007] obtain a shallower penetration of the horizontal near-inertial energy, probably because of the different N^2-profile used. They did not find a clear selective trapping of near-inertial energy within anti-cyclonic eddies, which is explained by the competition between lower and higher modes when the latter are resolved (see section 4). However, anti-cyclonic structures still act as a conduit for draining near-inertial energy. As illustrated by Figure 3 the horizontal near-inertial energy penetrates deeper in anti-cyclonic structures than in cyclonic ones. The horizontal scales involved can be as small as 20 km. More interestingly, their results reveal a conspicuous deeper penetration of the vertical velocity variance associated with the near-inertial motions: the vertical profile of this variance displays a maximum at a depth of 1700 m!

The competition between the high-frequency wind energy flux through the ocean surface and the near-inertial energy flux leaving the mixed-layer to the deeper ocean has strong consequences on the mixing in the surface layers. Indeed if all the near-inertial energy is trapped within the mixed-layer, the excitation of the mixed-layer oscillator by winds with frequencies close to f would force resonance and lead to a significant mixed-layer deepening (as illustrated by the academic results of Figure 4). However, the eddy effects on the near-inertial motion propagation govern the corresponding energy flux at the mixed-layer base, which much reduces the mixed-layer deepening. The decaying time scale of the mixed-layer near-inertial energy, due to its propagation into the deeper layers, is estimated to be on the order of $3-8$ days [*D'Asaro*, 1995; *Van Meurs*, 1998]. However, we still lack however a precise quantification of this flux at the mixed-layer base, as argued by *Zhai et al.* [2005], and therefore of how much near-inertial energy is used for mixing the upper layers and how much for the deeper layers.

As found by *Danioux et al.* [2007], one important imprint of the high-frequency wind signal in presence of mesoscale eddies is on the vertical velocity field. To our knowledge very few studies have so far examined this characteristic. *Klein et al.* [2007a] also analyze the vertical velocity field in realistic numerical simulations of the North Atlantic Ocean with the Parallel Ocean Program (POP) model at $1/10^\circ$ and 40 vertical levels [e.g. *Smith et al.*, 2000; *Malone et al.*, 2003]. The oceanic field is forced by, either 6-hourly or daily averaged, winds from Qscat scatterometer (QSCAT) blended with winds from the National Center for Environmental Prediction (NCEP). The vorticity field associated with mesoscale eddies is shown in Plate 2. The signature of the Gulf Stream is clearly visible, but this plate mostly shows that the eddy field is also fully turbulent outside the Gulf Stream. Plate 3 shows the wind energy flux at the ocean surface with the 6-hourly QSCAT/NCEP blended winds (which was the best frequency

available). At this time two significant large-scale atmospheric storms are present in the North Atlantic. But this plate also reveals, superimposed on the signature of the atmospheric storms, much smaller-scale features principally associated with the small-scale structures of the eddy field. The vertical velocity fields in two simulations, one with the 6-hourly QSCAT/NCEP blended winds and the other one with the same winds but daily averaged, have been examined. With daily winds, the vertical velocity field (blue curve on Plate 4) is relatively weak. There is an increase near the bottom principally due to the topographic effects. With 6-hourly winds, the vertical velocity field (red curve on Plate 4) is totally different. It displays much larger amplitudes, a very large depth extension, as well as a conspicuous maximum at 2700 m, i.e. well away from the topographic effects. At that depth, the vertical velocity field reaches rms amplitudes on the order of 25 m per day at 2700 m and involves small-scale patterns (on the order of $40-50$ km).

A similar experiment has been repeated using a simulation (performed on the Earth Simulator with the Regional Ocean Modeling System (ROMS) model) of a turbulent eddy field (described in *Klein et al.* [2007b]) that results from the baroclinic instability of a large-scale jet in a β-plane channel with no topography. The resolution is much higher (2 km in the horizontal and 100 vertical levels). The ocean is forced by the same wind stress time series as that displayed in Figure 1. The two curves in Plate 5 show the profile of the vertical velocity variance obtained either with the instantaneous wind forcing (red curve) or with the same wind forcing but daily average (blue curve). Again the presence of the high-frequency winds leads to a strong increase of the vertical velocity and the emergence of a significant maximum in the deep interior (at a depth of 2500 m with a rms value of 45 m per day!). On the other hand, when the wind is daily averaged, the vertical velocity is very much weaker with no clear maximum in the deep interior.

The appearance of the deep maximum of the vertical velocity is fully explained by *Danioux et al.* [2007]. It is principally due to the interacting mesoscale eddies that trigger a quick phase decoupling between the lower baroclinic modes of the near-inertial energy and the higher baroclinic modes. As a result the upper maximum on the red curve of Plate 5 is captured by the higher baroclinic modes whereas the deeper maximum is captured by the lower modes. The similitude of the deep maximum locations in Plates 4 and 5 is a coincidence since characteristics of the corresponding experiments are somewhat different. The depth of the maximum in the interior is actually sensitive to the representation of the higher modes and to the existence of vorticity structures at small-scale. Indeed the same experiment as that leading to the results shown on Plate 5 but with a lower resolution (6 km in the horizontal and 50 vertical levels) has produced a maximum at a depth of only 1700 m. Existence of this deep maximum is strong evidence that the presence of mesoscale eddies and sub-mesoscale structures opens an efficient pathway for the wind energy to go deep into the ocean interior where it could be available for mixing.

Another comment on these results is that in such turbulent eddy fields, the vorticity gradients have a rms value as large as 10^{-10}-10^{-9} $\mathrm{m}^{-1}\mathrm{s}^{-1}$, i.e. one to two orders of magnitude larger than the β-value ($\approx 1.6 * 10^{-11}$ $\mathrm{m}^{-1}\mathrm{s}^{-1}$ at mid-latitudes). This means that the dynamic related to the turbulent eddy field strongly dominates that due to the β-effect. Therefore near-inertial motions appear to be mostly trapped in the turbulent eddy field and can weakly propagate equatorward.

One question still to be adressed is: can these near-inertial motions efficiently cascade through the local wave number spectrum down to small dissipation scales? Usually PSI is the mechanism invoked for such a cascade, but it can only transfer energy from low-vertical mode double-inertial motions to small-scale inertial waves where dissipation occurs [e.g. *Hibiya et al.*, 1998;

Staquet and Sommeria, 2002]. This means that only near-inertial waves (with frequency very close to f) generated at mid-latitudes that propagate equatorward can cascade down through PSI at latitudes not larger than $\approx 30^\circ$ where the local Coriolis frequency is half that at mid-latitudes. However, it was found recently and confirmed in high-resolution simulations that the dominant frequency of the wind-driven vertical motions present in the deep ocean interior at mid-latitudes (Plates 4 and 5) is not close to f but is close to (and even over) $2f$, i.e. twice the Coriolis frequency (see Plate 6). The emergence of such supra-inertial motions (also reported in some observations such as those of *Mori et al.* [2005]) is due to a resonance mechanism described in *Danioux and Klein* [2007]. It therefore makes PSI a likely mechanism to convert vertical kinetic energy into mixing in the deep interior at these mid-latitudes. It is premature to produce any estimation of the corresponding mixing since PSI cannot be efficiently activated in a primitive-equation model. But this result indicates the existence of a significant source of low-vertical-mode internal waves with frequency equal or over $2f$ at mid-latitudes. Such a result emphasizes the strong potentiality of wind-driven near-inertial motions to significantly contribute to the mixing in the deep ocean interior.

7. Eddy-resolving models and high-frequency winds: what resolution is needed?

Our hypothesis is that eddy-resolving models at a basin scale can be very helpful to address the questions still unanswered about the precise contribution of the different pathways by which near-inertial motions propagate. The eddy-resolving models should allow a particular understanding of how much of the large amount of energy provided by high-frequency winds is available for mixing in both the upper layers and the deep interior and at which latitudes. The prerequisite is to have access to realistic high-frequency winds and to use numerical models at a basin scale with adequate spatial resolution.

High-frequency intermittent winds are usually linked with fast travelling atmospheric fronts associated with storms. Atmospheric fronts are narrow (with a width of $\mathcal{O}(100$ km)) and elongated on a long distance (more than 1000 km). The atmospheric fronts have a strong signature on the relative vorticity, which explains the strong and rapid variation of both the wind amplitude and direction when they pass over the ocean surface at a given location. NCEP or European Center for Medium Range Weather Forecasting (ECMWF) data cannot represent such features because of their spatial resolution (involving spatial grid equal or larger than 100 km).

However when these data are blended with data from satellite scatterometers, such as QSCAT and ADEOS-II scatterometers, time variation of the amplitude and rotation of the high-frequency winds are much better represented (e.g. http://www.cora.nwra.com/morzel/). This is illustrated in Plate 7, which shows the atmospheric vorticity field near the surface estimated from only the NCEP data (upper panel) and from blended winds generated with only QSCAT (middle panel) and with both QSCAT and ADEOS-II data (lower panel). Results show that fronts and storms are very much better resolved when NCEP data are blended with scatterometer data. The propagation of fronts and storms, and therefore the intermittency of the winds, are better represented when using two scatterometers instead of one (compare the three panels in Plate 7). With two scatterometers the blending window can be reduced from 12 hr to 7.5 hr; i.e. every 6-hourly NCEP global field is blended with 7.5 hr each of QSCAT and ADEOS-II data. Such data, when they are available, strongly improve the spatial and time intermittency of the high-frequency winds [e.g. *Milliff et al.*, 2004; *Chelton et al.*, 2004], which highlights the strong value and potentiality of high-resolution scatterometers.

Eddy-resolving models at a basin scale should have adequate horizontal and vertical resolution in order to be able to represent the 3-D propagation of the wind-driven near-inertial energy.

This means a horizontal resolution involving a horizontal space grid equal to or less than 3 km and a vertical resolution with at least 100 levels. Two reasons advocate for the use of such spatial resolution.

First, as noted before, the vertical propagation of near-inertial waves down to 4000 m depth results from the phase decoupling of the lower and higher baroclinic modes. Higher baroclinic modes have a Rossby radius of deformation on the order of a few kilometers. This requires a space grid not larger than 3 km and a vertical resolution involving at least 100 levels on the vertical in order to resolve these Rossby radii (multiplied by 2π) and to correctly represent the rapid variation with depth of these vertical modes.

The second reason is that the surface dynamics driven by the mesoscale eddy turbulence involves quite small spatial scales or sub-mesoscale structures, with scales as small as 5 km, that need to be explicitly resolved. The energetic character of these sub-mesoscale structures is emphasized by high-resolution simulations of such eddy turbulence [e.g. *McWilliams et al.*, 2004; *Capet et al.*, 2007a, b, c; *Klein et al.*, 2007b] that exhibit a k^{-2} velocity spectrum in the surface layers. Frontogenesis underlies the physics involved and explains the small-scale structures in Plate 8 with large relative vorticity values. Dynamics of these sub-mesoscale structures are documented in *Mahadevan* [2006], *Mahadevan and Tandon* [2006], and *Thomas et al.* [2007].

As mentioned before, these sub-mesoscale structures have a significant impact on the 3-D propagation of the near-inertial energy (and therefore on the depth of the maximum in the interior), but also on the resulting mixing in both the upper layers and the deep interior. Indeed, they drive a strong restratification in the upper layers, compensated for by a destratification in the ocean interior [e.g. *Lapeyre et al.*, 2006; *Klein et al.*, 2007b]. Such restratification competes with the mixed-layer dynamics [e.g. *McWilliams*, 2007]. On the other hand, the wind

forcing itself can affect these sub-mesoscale structures as explicitly shown by *Thomas* [2005], *Thomas and Lee* [2005], *Giordani and Caniaux* [2006], *Boccaletti et al.* [2007] and *Thomas et al.* [2007]. All these mechanisms should have a non-negligeable impact on the resulting mixing by both the near-inertial waves and the sub-mesoscale structures in the upper oceanic layers. At last they have a significant effect on the phase decoupling between lower and higher modes of the near-inertial motions, and therefore on the vertical propagation of these motions, since the higher modes dispersion is strongly sensitive to the presence and amplitude of these sub-mesoscale structures [e.g. *Klein et al.*, 2004b].

Characteristics of the deep maximum of vertical velocity variance observed at $2500-3000$ m, as found by *Danioux et al.* [2007] and other studies, make the PSI a likely mechanism to convert the vertical kinetic energy into vertical turbulent diffusion [e.g. *Staquet and Sommeria*, 2002; *Koudella and Staquet*, 2006]. As such the deep maximum of high-frequency motions can potentially participate to the vertical mixing in this region. A very rough scaling analysis (using $K_z \approx < w^2 > / f$) indicates that, even if only 10% of the near-inertial vertical kinetic energy is converted into energy available for mixing through PSI, the corresponding value (10^{-4} m^{2}s^{-1}) would be much larger than the 10^{-6} m^{2}s^{-1} molecular value and should be close to that necessary for mixing in the deep interior [e.g. *Wunsch and Ferrari*, 2004]. This comment calls for further studies on these mechanisms to fully evaluate the efficiency of PSI for the characteristics of the supra-inertial energy present in the deep interior. These studies could lead to development of an appropriate parameterization to convert this near-inertial energy at depth into mixing.

Within a climate change scenario these mechanisms that open a route to mixing from the surface to the deep ocean interior, suggest that the atmosphere, through the high-frequency winds, may affect the stratification and the MOC, i.e. the large-scale oceanic circulation. Recent re-

views [*Schiermeier*, 2007] and studies [*Sriver and Huber*, 2007; *Emmanuel*, 2001] have already pointed out that tropical cyclones (or hurricanes) mix the upper ocean so well that they are responsible for a staggering amount of heat transfer on a global scale. This means that within an extreme climate scenario, an increase of tropical cyclone power and frequency (due to future changes in tropical sea surface temperature) may accelerate the MOC. This might feed back on climate by redistributing heat poleward and therefore raising global mean temperature [*Sriver and Huber*, 2007]. On the other hand, the mechanisms reviewed in this paper suggest in the same way that an increase of the strength and intensity of the extra-tropical atmospheric storms may be accompanied by a strengthened MOC and/or an intensified eddy kinetic energy at mid-latitudes with the same climate consequences. However, these effects at mid-latitudes would be efficient on a larger depth than those due to tropical cyclones. All these features, which still have to be quantified, emphasize the need to explicitly take into account the small scales of the atmospheric and oceanic dynamics in order to understand the coupled atmosphere-ocean system at larger scales.

Acknowledgments. Contributions from and discussions with Eric Danioux, Matthew Hecht, Guillaume Lapeyre, Bill Large, and Nobu Komori during the preparation of this short review are greatly acknowledged. This work is supported by the Institut Francais de Recherche pour l'Exploitation de la Mer (IFREMER) and the Centre National de la Recherche Scientifique (CNRS), FRANCE. Some numerical simulations reported here were done on the Earth Simulator (Yokohama, Japan), the access to which has been made possible through a memorandum of understanding between the IFREMER, the CNRS, and the Earth Simulator Center/Japan Agency for Marine-Earth Science and Technology (ESC/JAMSTEC). The support from the

French ANR (Agence Nationale pour la Recherche, Contract No. ANR-05-CIGC-010) is also acknowledged. At last, the referees are thanked for their constructive comments.

Notes

1. Any motion can be decomposed into vertical normal modes that are solutions of a Sturm-Liouville problem [e.g. *Gill*, 1984], which only requires the knowledge of the vertical stratification. Each mode is associated with a Rossby radius of deformation whose value at mid-latitudes ranges from ≈ 50 km for the lower modes to $\approx 2-3$ km for the higher modes. So equation (1) can be seen as the dispersion relation associated with one vertical mode.

References

Alford, M. H. (2001), Internal swell generation: the spatial distribution of energy flux from the wind to mixed-layer near-inertial motions, *J. Phys. Oceanogr.*, *31*, 2359–2368.

Alford, M. H. (2003), Improved global maps and 54-year history of wind-work on ocean inertial motions, *Geophys. Res. Lett.*, *30(8)*, L1424, doi:10.1029/2002GL016,614.

Assenbaum, M., and G. Reverdin (2005), Near-real time analyses of the mesoscale circulation during the pomme experiment., *Deep-Sea Res.*, *30*, 2343–2353.

Balmforth, N., S. L. Smith, and W. Young (1998), Enhanced dispersion of near-inertial waves in an idealized geostrophic flow, *J. Mar. Res.*, *56*, 1–40.

Boccaletti, G., R. Ferrari, and B. Fox-Kemper (2007), Mixed layer instabilities, *J. Fluid Mech.*, in press.

Capet, X., J. C. McWilliams, M. Molemaker, and A. Shchepetkin (2007a), Mesoscale to submesoscale transition in the california current system. Part 1: Flow structure and eddy flux, *J. Phys. Oceanogr.*, in press.

Capet, X., J. C. McWilliams, M. Molemaker, and A. Shchepetkin (2007b), Mesoscale to submesoscale transition in the california current system, Part 2: Dynamical processes and obser-

vational tests, *J. Phys. Oceanogr.*, in press.

Capet, X., J. C. McWilliams, M. Molemaker, and A. Shchepetkin (2007c), Mesoscale to submesoscale transition in the california current system. Part 3: Energy balance and flux, *J. Phys. Oceanogr.*, submitted.

Chelton, D., M. Schlax, M. Freilich, and R. Milliff (2004), Satellite measurements reveal persistent small-scale features in ocean winds, *Science*, *303*, 978–983.

Danioux, E., and P. Klein (2007), A resonance mechanism leading to wind-forced supra-inertial motions with a $2f$ frequency, *J. Phys. Oceanogr.*, in revision.

Danioux, E., P. Klein, and P. Rivière (2007), Propagation of wind energy into the deep ocean through mesoscale eddies, *J. Phys. Oceanogr.*, in revision.

D'Asaro, E. A. (1989), The decay of wind-forced mixed layer inertial oscillations due to the β-effect, *J. Geophys. Res.*, *94*, 2045–2056.

D'Asaro, E. A. (1995), Upper-ocean inertial currents forced by a strong storm. Part iii: Interaction of inertial currents and mesoscale eddies, *J. Phys. Oceanogr.*, *25*, 2953–2958.

Emmanuel, K. (2001), Contribution of tropical cyclones to meridional heat transport by the oceans, *J. Geophys. Res.*, *D14*, 14,771–14,781.

Garrett, C. (2001), What is the "near inertial" band and why is it different from the rest of the internal wave spectrum?, *J. Phys. Oceanogr.*, *31*, 962–971.

Gill, A. (1984), On the behavior of internal waves in the wakes of storms, *J. Phys. Oceanogr.*, *14*, 1129–1151.

Giordani, L. P., and G. Caniaux (2006), Advanced insights into sources of vertical velocity in the ocean, *Ocean Dynamics*, *56*, 513–524.

Hibiya, T., Y. Niwa, and K. Fujiwara (1998), Numerical experiments of nonlinear energy transfer within the oceanic internal wave spectrum, *J. Geophys. Res.*, *103*, 18,715–18,722.

Hibiya, T., M. Nagasawa, and Y. Niwa (1999), Model predicted distribution of internal wave energy for diapycnal mixing processes in the deep waters of the North Pacific., in *Dynamics of oceanic internal gravity waves: Proc. AhaHulikoa Hawaiian Winter Workshop*, pp. 205–215, P. Müller and D. Henderson. Hawaii Institute of Geophysics.

Hurlburt, H. E., and P. J. Hogan (2000), Impact of $1/8^\circ$ to $1/64^\circ$ resolution on gulf stream model-data comparisons in basin-scale subtropical atlantic ocean models, *Dyn. Atm. Oc.*, *32*, 283–329.

Klein, P. (1990), Transition to chaos in unstable baroclinic systems: a review, *Fluid Dyn. Res.*, *5*, 235–254.

Klein, P., and M. Coantic (1981), A numerical study of turbulent processes in the marine upper layers, *J. Phys. Oceanogr.*, *11*, 849–863.

Klein, P., and A. Tréguier (1995), Dispersion of wind-induced inertial waves by a barotropic jet., *J. Mar. Res.*, *53*, 1–22.

Klein, P., G. Lapeyre, and W. G. Large (2004a), Wind ringing of the ocean in presence of mesoscale eddies, *Geophys. Res. Lett.*, *31*, L15,306, doi:10.1029/2004GL020,274.

Klein, P., S. Llewellyn-Smith, and G. Lapeyre (2004b), Spatial organisation of inertial energy by an eddy field, *Q. J. R. Meteorol. Soc.*, *130*, 1153–1166.

Klein, P., M. Hecht, W. Large, and E. Danioux (2007a), Propagation of high-frequency wind energy in the deep oceanic interior through mesoscale eddies, *Geophys. Res. Lett.*, submitted.

Klein, P., B. Hua, G. Lapeyre, X. Capet, S. L. Gentil, and H. Sasaki (2007b), Upper ocean turbulence form high 3-d resolution simulations, *J. Phys. Oceanogr.*, in press.

Komori, N. (2007), Personal communication. Earth Simulator Center, Yokohama, Japan.

Koudella, C., and C. Staquet (2006), Instability mechanisms, *J. Fluid Mech., 548*, 165–196.

Kunze, E. (1985), Near-inertial wave propagation in geostrophic shear, *J. Phys. Oceanogr.*, *15*, 544–565.

Lapeyre, G., P. Klein, and B. L. Hua (2006), Oceanic restratification by surface frontogenesis, *J. Phys. Oceanogr., 36*, 1577–1590.

Large, W. G., and G. B. Crawford (1995), Observations and simulations of upper-ocean response to wind events during the ocean storms experiment, *J. Phys. Oceanogr.*, *25*, 2831–2852.

LeCann, B., M. Assenbaum, J. Gascard, and G. Reverdin (2005), Observed mean and mesoscale upper ocean circulation in the mid-latitude northeast Atlantic, *J. Geophys. Res.*, *110 (C7)*, C07S05 10.1029/2004JC002,768.

Lee, D.-K., and P. P. Niiler (1998), The inertial chimney: the near inertial energy drainage from the ocean surface to the deep layer, *J. Geophys. Res.*, *103 (C4)*, 7579–7591.

MacKinnon, J., and K. Winters (2005), Subtropical catastrophe: significant loss of low-mode tidal energy at 28.9°, *Geophys. Res. Lett.*, *32*, L15,605, doi:10.1029/2005GL023,376.

Mahadevan, A. (2006), Modeling vertical motion at ocean fronts: Are non-hydrostatic effects relevant at sub-mesoscales?, *Ocean Modelling*, *14*, 222–240.

Mahadevan, A., and A. Tandon (2006), An analysis of mechanisms for sub-mesoscale vertical motions at ocean fronts, *Ocean Modelling*, *14*, 241–256.

Malone, R., R. Smith, R. Maltrud, and M. Hecht (2003), Eddy-resolving ocean modeling, *Los Alamos Science*, *28*, 223–231.

McWilliams, J. (2007), On the role of eddies, in *Eddy Resolving Models*, AGU.

McWilliams, J., M. Molemaker, and I. Yavneh (2004), Ageostrophic, anticyclonic instability of a barotropic boundary current, *Phys. Fluids*, *16*, 3720–3725.

Milliff, R., R.F., J. Morzel, D. Chelton, and M. Freilich (2004), Wind stress curl and wind stress divergence biases from rain effects on qscat surface wind retrievals, *J. Atmos. Ocean. Tech.*, *21*, 1216–1231.

Mori, K., T. Matsuno, and T. Senjyu (2005), Seasonal/spatial variations of the near-inertial oscillations in the deep water of the japan sea, *J. Oceanogr.*, *61*, 761–773.

Munk, W., and C. Wunsch (1998), Abyssal recipes ii: energetics of tidal and wind mixing, *Deep-Sea Res.*, *45*, 1976–2009.

Nagasawa, M., Y. Niwa, and T. Hibiya (2000), Spatial and temporal distribution of wind-induced internal wave energy available for deep water mixing in the north pacific, *J. Geophys. Res.*, *105*, 13,933–13,943.

Price, J. (1981), Upper ocean response to a hurricane, *J. Phys. Oceanogr.*, *11*, 153–175.

Price, J., T. Sanford, and G. Forristall (1994), Forced stage response to a moving hurricane, *J. Phys. Oceanogr.*, *24*, 233–260.

Rudnick, D. L. (2001), On the skewness of vorticity in the upper ocean, *Geophys. Res. Lett.*, *28*, 2045–2048.

Sasaki, H. (2007), Personal communication. Earth Simulator Center, Yokohama, Japan.

Schiermeier, Q. (2007), Churn, churn, churn, *Nature*, *477*, 522–524.

Siegel, A., J. B. Weiss, J. Toomre, J. C. McWilliams, P. S. Berloff, and I. Yavneh (2001), Eddies and vortices in ocean basin dynamics, *Geophys. Res. Lett.*, *28*, 3183–3186.

Skyllinstad, E., W. Smyth, and G. Crawford (2000), Resonant wind-driven mixing in the ocean boundary layer, *J. Phys. Oceanogr.*, *30*, 1866–1890.

Smith, R., M. Maltrud, F. Bryan, and M. Hecht (2000), Numerical simulation of the North Atlantic Ocean at 1/10°, *J. Phys. Oceanogr., 30*, 1532–1561.

Sriver, R., and M. Huber (2007), Observational evidence for an ocean heat pump induced by tropical cyclones, *Nature, 447*, 577–580.

Stammer, D. (1997), Global characteristics of ocean variability estimated from regional TOPEX/POSEIDON altimeter measurements, *J. Phys. Oceanogr., 27*, 1743–1769.

Stammer, D., and C. Wunsch (1999), Temporal changes in eddy energy of the oceans, *Deep-Sea Res., 46*, 77–108.

Staquet, C., and J. Sommeria (2002), Internal gravity waves: from instabilities to turbulence, *Annu. Rev. Fluid Mech., 34*, 559–593.

Stockwell, R., W. Large, and R. Milliff (2004), Resonant inertial oscillations in moored buoy ocean surface winds, *Tellus, 56*, 536–547.

Thomas, L. N. (2005), Destruction of potential vorticity by winds, *J. Phys. Oceanogr., 35*, 2457–2466.

Thomas, L. N., and C. M. Lee (2005), Intensification of ocean fronts by down-front winds, *J. Phys. Oceanogr., 35*, 1086–1102.

Thomas, L. N., A. Tandon, and A. Mahadevan (2007), Submesoscale processes and dynamics, in *eddy resolving models*, AGU.

Van Meurs, P. (1998), Interactions between near-inertial mixed layer currents and the mesoscale: the importance of spatial variabilities in the vorticity field, *J. Phys. Oceanogr., 28*, 1363–1388.

Watanabe, M., and T. Hibiya (2002), Global estimates of the wind-induced energy flux to inertial motions in the surface mixed layer, *Geophys. Res. Lett., 29*, 80–1–80–4.

Weller, R. (1982), The relation of near-inertial motions observed in the mixed layer during the JASIN (1978) experiment to the local wind stress and the quasigeostrophic flow field, *J. Phys. Oceanogr.*, *12*, 1122–1136.

Wunsch, C. (1998), The work done by the wind on the oceanic general circulation, *J. Phys. Oceanogr.*, *28*, 2332–2340.

Wunsch, C., and R. Ferrari (2004), Vertical mixing, energy and the general circulation of the ocean, *Annu. Rev. Fluid Mech.*, *36*, 281–314.

Young, W., and M. Ben Jelloul (1997), Propagation of near-inertial oscillations through a geostrophic flow, *J. Mar. Res.*, *55*, 735–766.

Zhai, X., R. J. Greatbach, and J. Zhao (2005), Enhanced vertical propagation of storm-induced near-inertial energy in an eddying ocean channel model, *Geophys. Res. Lett.*, *32*, L18,602.

Table 1. Statistics over 540 days of the near-inertial energy integrated over the water column (in $m^3 s^{-2}$) obtained with the 1-D model (from *Klein et al.* [2004a]).

Simulations	**3-hourly winds**	**6-hourly winds**	**12-hourly winds**	**24-hourly winds**
Near-inertial energy				
Mean value	2.03	1.65	0.62	0.28
RMS value	1.70	1.38	0.56	0.28

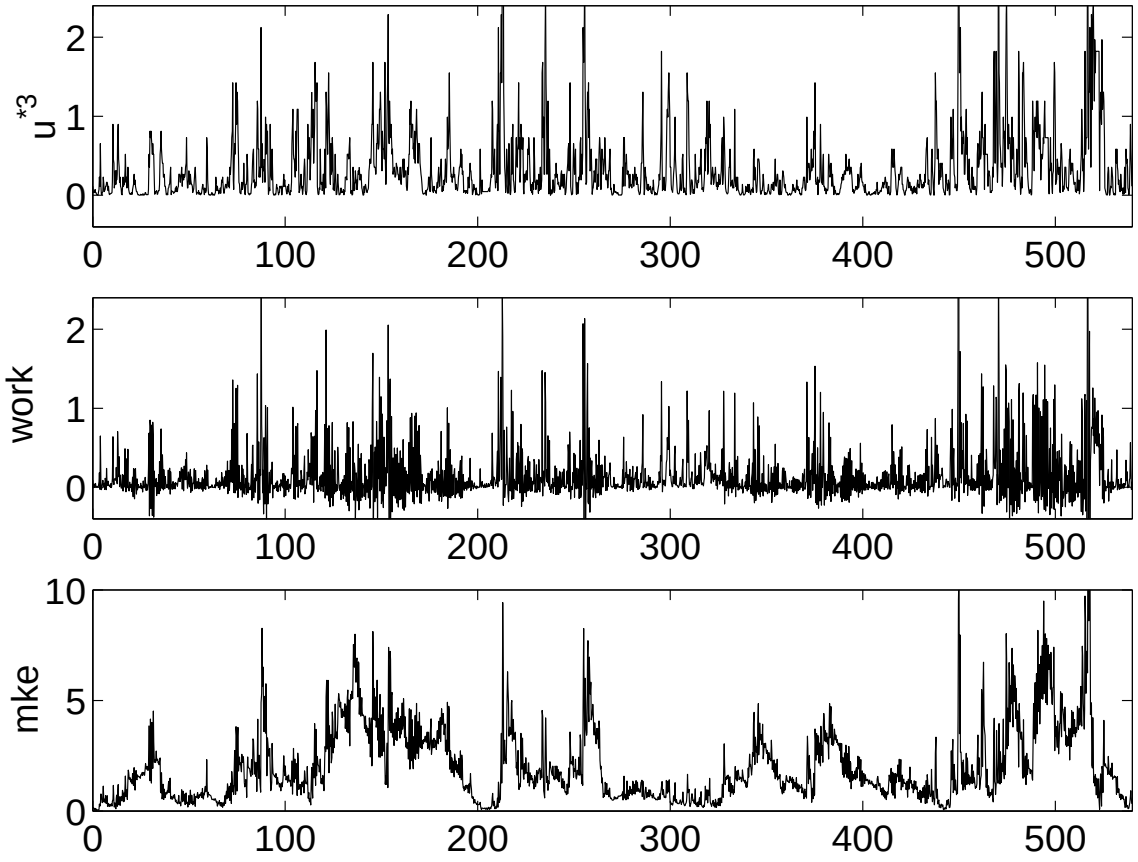

Figure 1. Results (from *Klein et al.* [2004a]) of a 3-hourly simulation using a Mellor and Yamada model and a real wind time series. (upper panel) $u^{*3} = |\boldsymbol{\tau}|^{\frac{3}{2}}$ (in m^3 s$^{-3}\times 1.5\cdot 10^5$), (middle panel) wind energy flux ($[\boldsymbol{\tau} \cdot \mathbf{u}]$(in m^3 s$^{-3}\times 10^4$)), (lower panel) inertial energy integrated over the water column (in m^3 s^{-2}). Abscissa units are days.

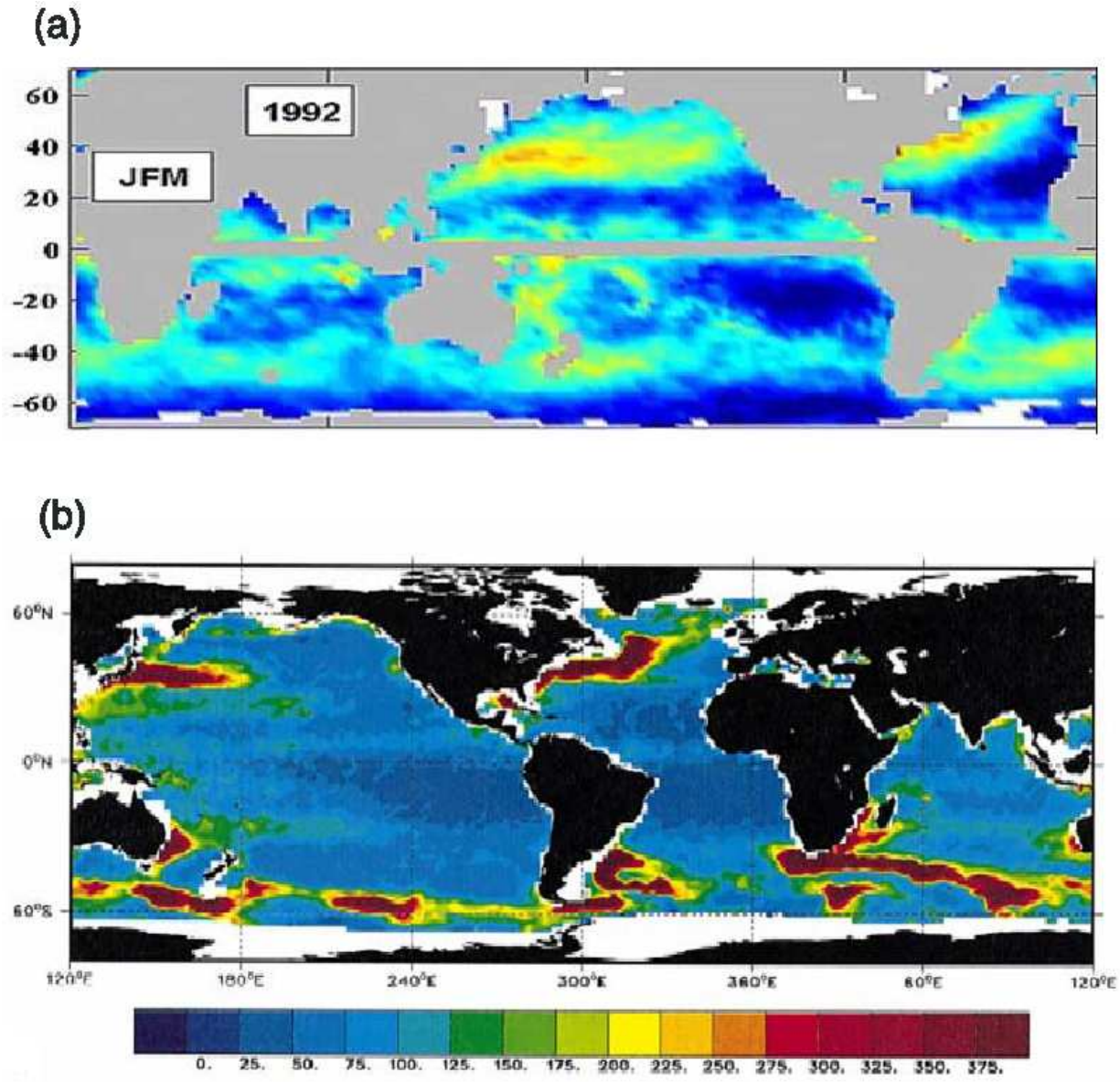

Plate 1. (a) Near-inertial energy input at the ocean surface in the winter season (from *Alford* [2003]) and (b) Mesoscale eddy kinetic energy in the upper oceanic layers (from *Stammer and Wunsch* [1999]). Reproduced from *Zhai et al.* [2005].

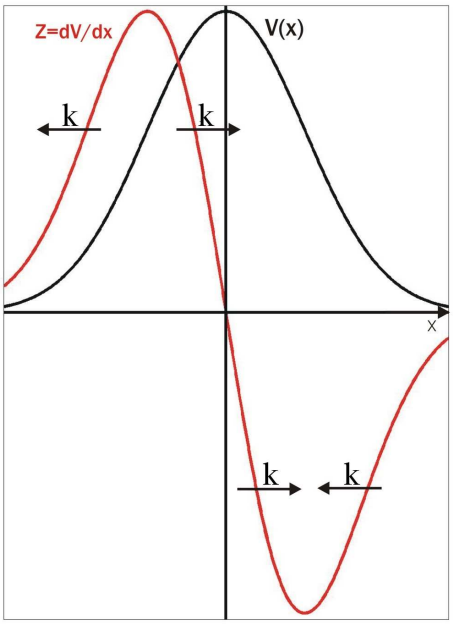

Figure 2. Schematic representation of the propagation of near inertial waves induced by a one dimensional jet V(x). The velocity V(x) and the vorticity $Z = \frac{\partial V}{\partial x}$ are shown. The wave numbers $k = -\frac{\partial Z}{\partial x}\frac{t}{2}$ are represented by black arrows.

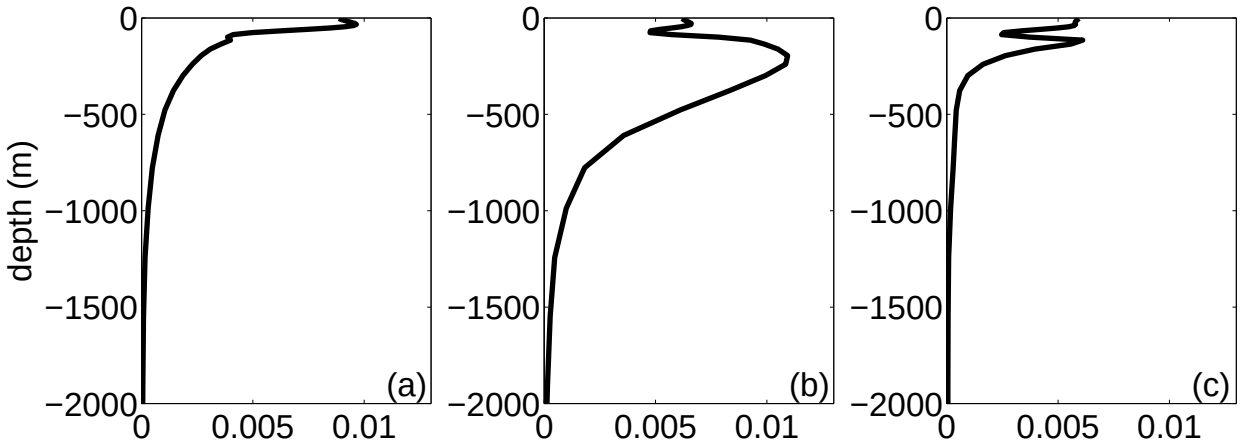

Figure 3. Vertical profiles of the horizontal near-inertial energy (a) averaged over the whole domain, (b) averaged over negative vorticity areas (corresponding to $Z < -2.10^{-5}s^{-1}$), and (c) averaged over positive vorticity areas (corresponding to $Z > 2.10^{-5}s^{-1}$). From *Danioux et al.* [2007].

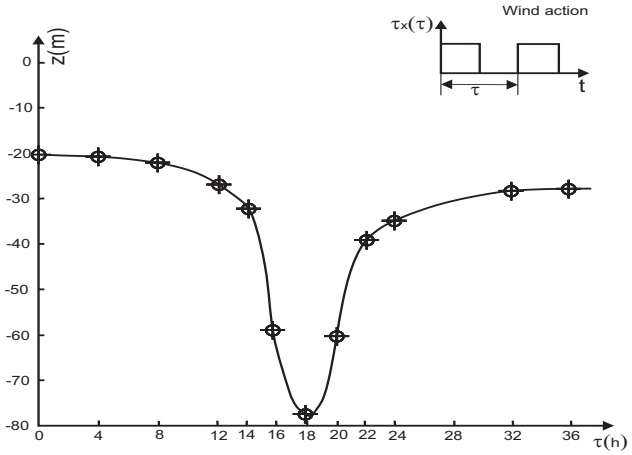

Figure 4. Mixed-layer depth after a 4-day academic simulation in terms of the time period T (in hours) of the wind forcing (from *Klein and Coantic* [1981]). Coriolis frequency is $f = 10^{-4}\mathrm{s}^{-1}$ ($[18h]^{-1}$).

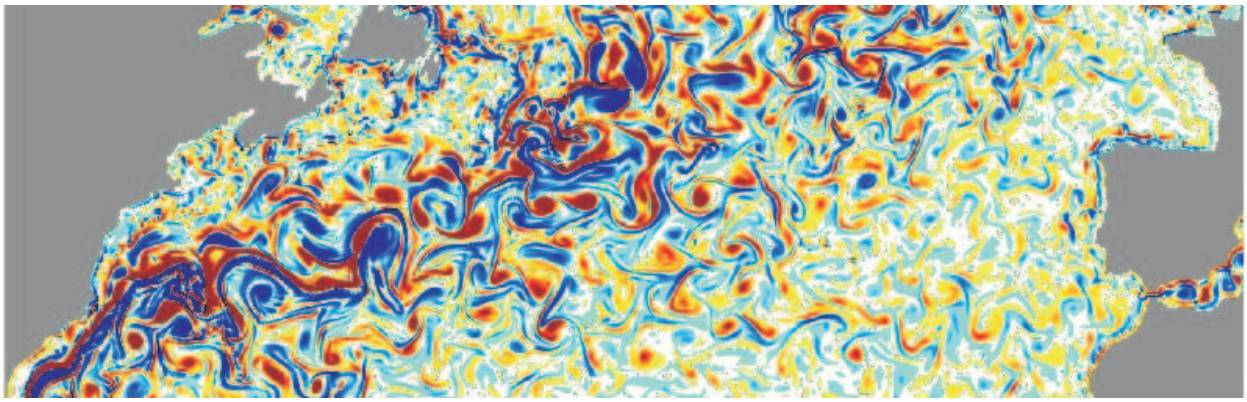

Plate 2. Surface vorticity field in the North Atlantic in January 2002. This field has been obtained from a simulation with the POP model at 1/10° [e.g. *Smith et al.*, 2000].

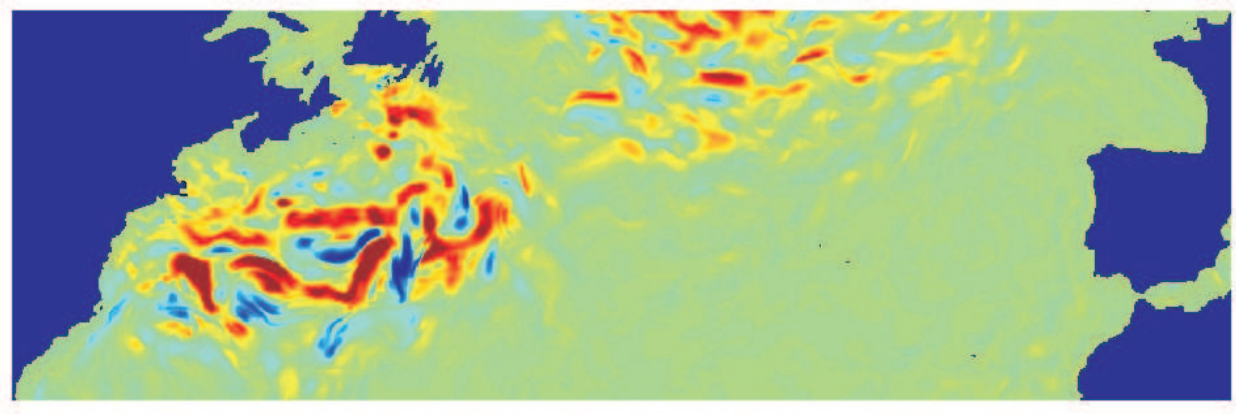

Plate 3. Wind energy input ($[\boldsymbol{\tau} \cdot \mathbf{u}]$) to the North Atlantic Ocean in January 2002 (simulated with the POP model (see Plate 2)) using 6-hourly QSCAT/NCEP blended wind data. From *Klein et al.* [2007a].

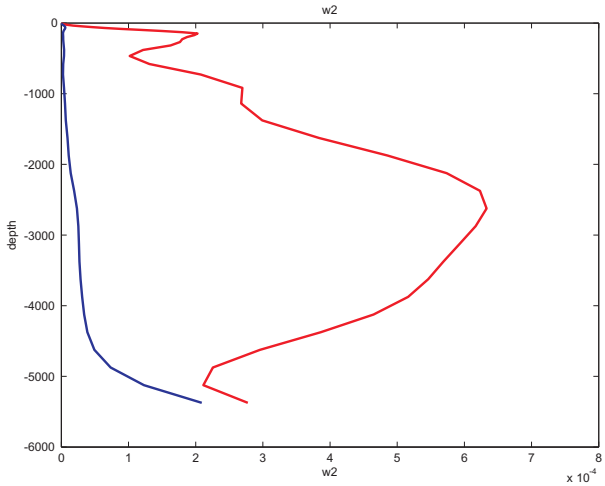

Plate 4. Vertical profiles of the vertical velocity variance in the POP simulation, using a wind forcing with 6-hourly QSCAT/NCEP blended wind data (red curve) and when the wind forcing is averaged over 24 hours (blue curve). From *Klein et al.* [2007a].

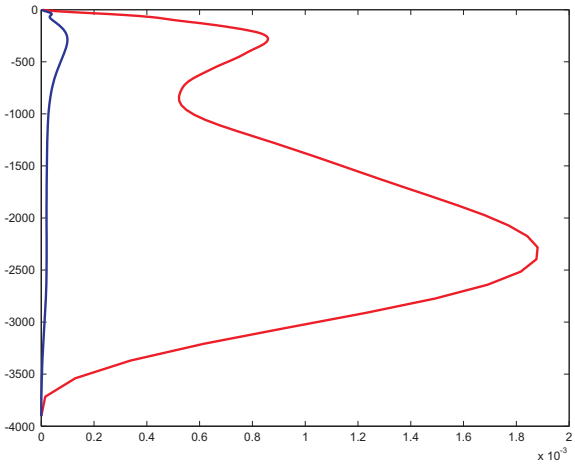

Plate 5. Vertical profiles of the vertical velocity variance in a simulation performed on the Earth Simulator [*Klein et al.*, 2007b], using the real 3-hourly wind time series of *Klein et al.* [2004a] (red curve) and when this wind time series is averaged over 24 hours (blue curve).

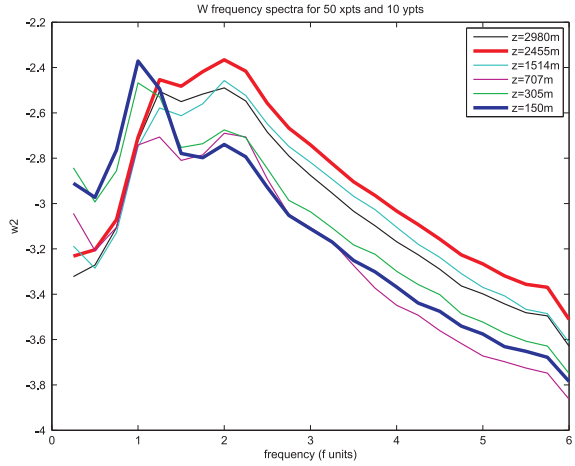

Plate 6. Frequency spectra of the vertical velocity variance at different depths from the Earth Simulator simulation [*Klein et al.*, 2007b], using a real 3-hourly wind time series. Frequencies on the horizontal axis are non-dimensionalized by f. The dominant frequency at 150 m is f, but it is $2f$ at 2455 m and 2980 m.

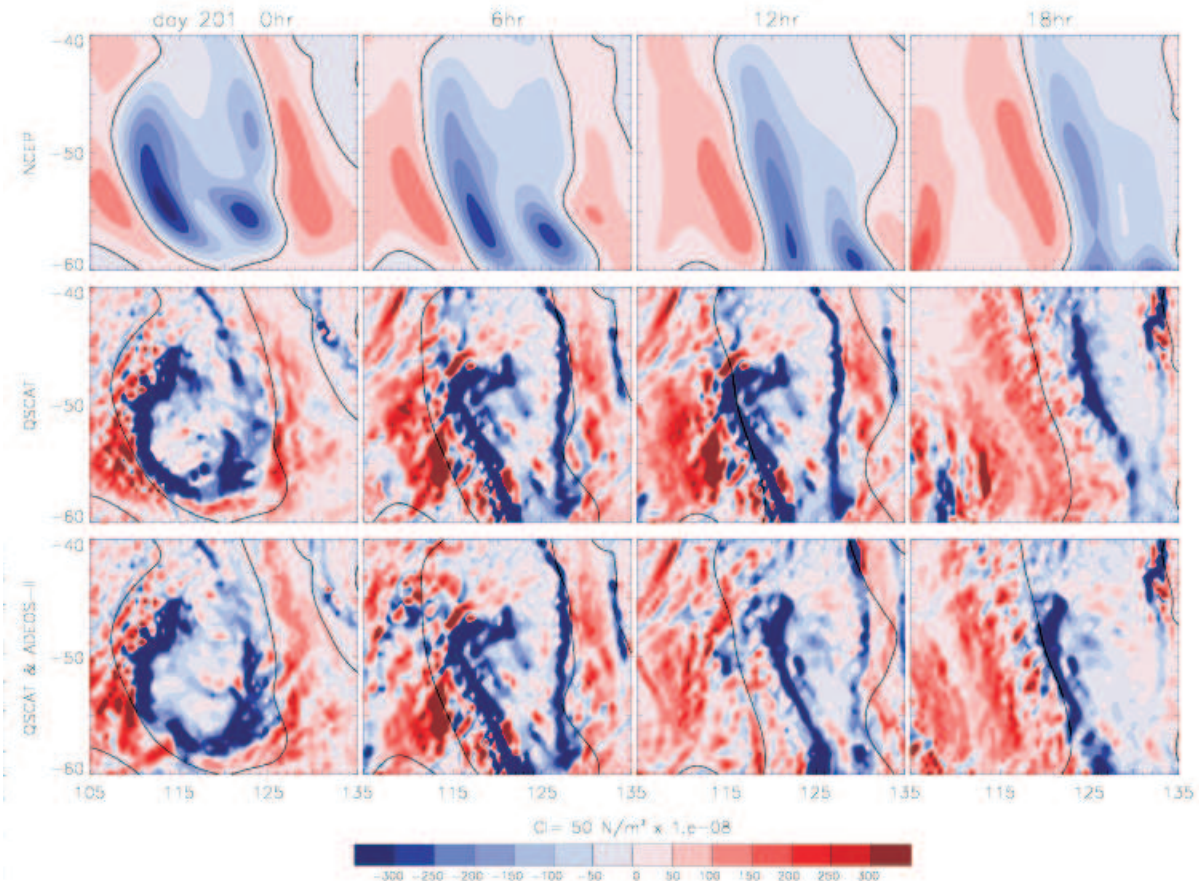

Plate 7. The 6-hourly time sequence of the wind stress curl (at $40°-60°$S, $75°-135°$E) estimated from only the NCEP data (upper panel), from blended winds generated with QSCAT only (middle panel) and with both QSCAT and ADEOS-II data (lower panel). See http://www.cora.nwra.com/ morzel/blendedwinds.qscat.swsa2.html. The dual-blended wind data agree very well with the location in NCEP, whereas the single-blended winds are already 6 hr ahead, placing the curl front too far to the East [e.g. *Milliff et al.*, 2004; *Chelton et al.*, 2004].

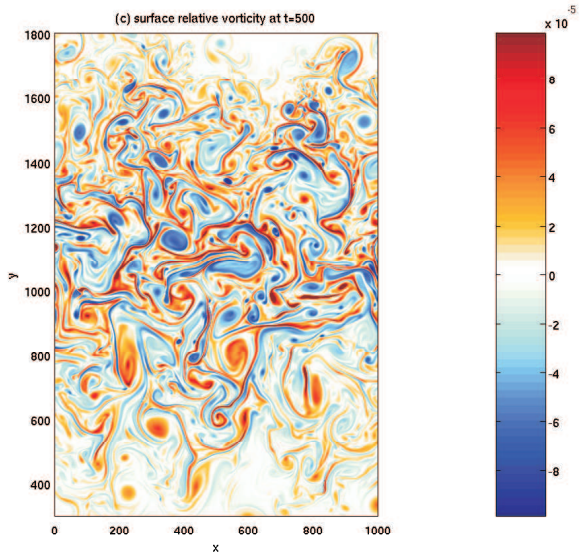

Plate 8. Snapshot of the surface relative vorticity field in a high resolution simulation (from *Klein et al.* [2007b]).